nature nanotechnology

SUPPLEMENTARY INFORMATION

DOI: 10.1038/NNANO.2014.336

Microwave-driven coherent operation of a semiconductor quantum dot charge qubit

Dohun Kim, D. R. Ward, C. B. Simmons, John King Gamble, Robin Blume-Kohout, Erik Nielsen, D. E. Savage, M. G. Lagally, Mark Friesen, S. N. Coppersmith, and M. A. Eriksson

SUPPLEMENTARY INFORMATION

S1. DETAILS OF TIME-AVERAGED MEASUREMENT AND PROBABILITY NORMALIZATION

For the measurement of changes in the probabilities of charge occupation resulting from fast microwave bursts, we use the general approach described in [1], where we measure the difference between the QPC conductance with and without the manipulation pulse train. Fig. S1 shows similar scheme adopted in this work. We alternate an appropriate number of manipulation and measurement sequences (measurement time ∼60 ns) with microwave bursts with adiabatic in and out sequences without microwaves to form a low frequency signal with frequency on the order of ∼1 kHz. The adiabatic ramp sequence without microwave manipulation does not induce state population change, but greatly reduces the background signal due to capacitive crosstalk. The manipulation sequence including the microwave bursts is generated using a Tektronix AWG70002A arbitrary waveform generator with a maximum sample rate of 25 Gs/s and an analog bandwidth of about 13 GHz. The data are acquired using a lock-in amplifier with a reference signal corresponding to the presence and absence of the pulses, as shown schematically by the orange dashed line in Fig. S1. We compare the measured signal level with the corresponding $(2,1)$-$(1,2)$ charge transition signal level, calibrated by sweeping gate GL and applying the orange square pulse shown in Fig. S1 to gate GL. Similarly to previous work [1], charge relaxation during the measurement phase is taken into account using the measured charge relaxation time $T_1 \approx 23.5$ ns at the read-out detuning of $\delta\varepsilon_r \approx -160$ μeV.

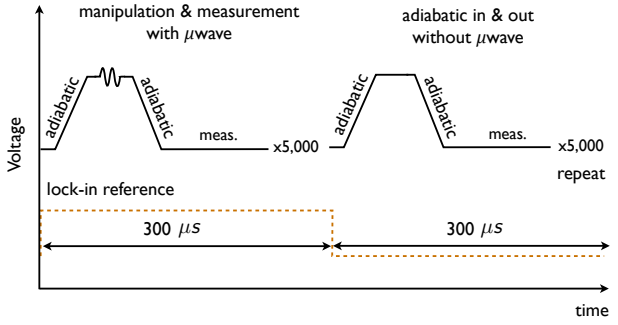

Supplementary Fig. S1. Pulse sequence used for lock-in measurement of the qubit state. The orange dashed line shows the corresponding lock-in reference signal, which also serves as the probability calibration pulse.

S2. ESTIMATE OF INITIALIZATION AND READOUT FIDELITY

During initialization, the qubit is transformed from $|L\rangle$ to $|0\rangle$ by ramping the detuning from the initialization/readout point to the sweet spot, and during readout the detuning is ramped from the sweet spot back to the initialization/readout point. Here, we characterize the infidelity in the initialization and readout processes from nonadiabaticity of the dynamics and from charge relaxation.

A. Numerical calculation of infidelity from nonadiabaticity.

Infidelity arising from nonadiabiticity is estimated by direct integration of the quantum mechanical evolution of the system using values for the Hamiltonian parameters obtained from experiment. The energy level diagram of Fig. 1c is calculated from the Hamiltonian written in the basis of the ground and first excited states of the electron charge states $(2,1) = |L\rangle$ and $(1,2) = |R\rangle$: $\{|L\rangle_{\rm g}, |L\rangle_{\rm e}, |R\rangle_{\rm g}, |R\rangle_{\rm e}\}$. In this basis, H is given by

$$H = \begin{pmatrix} \varepsilon/2 & 0 & \Delta_1 & -\Delta_2 \\ 0 & \varepsilon/2 + \delta E_{\rm L} & -\Delta_3 & \Delta_4 \\ \Delta_1 & -\Delta_3 & -\varepsilon/2 & 0 \\ -\Delta_2 & \Delta_4 & 0 & -\varepsilon/2 + \delta E \end{pmatrix}. \quad \text{(S1)}$$

Here, Δ_{1-4} are tunnel coupling matrix elements, ε is the detuning energy, and $\delta E_{\rm L}$ and δE are the energy separations of the ground and excited $|L\rangle$ and $|R\rangle$ states, respectively. The parameters Δ_3, Δ_4, and $\delta E_{\rm L}$ are relevant to high energy states which are not accessed experimentally in this work, and we use the values determined from our previous study [2]. We use parameters of tunnel coupling between $|L\rangle$ and $|R\rangle$ $2\Delta_1/h = 5.2$ GHz, tunnel coupling between $|L\rangle$ and low lying excited state $|R\rangle_{\rm e}$ on the right dot $2\Delta_2/h = 14.5$ GHz, and singlet-triplet energy splitting on the right dot $\delta R = 12.1$ GHz, extracted from measurements as in Refs. [1, 2]. To use the Hamiltonian of Eq. (S1) to estimate the effects of nonadiabaticity in reducing the fidelity of state initialization and measurement, we model the dynamical evolution of the density matrix ρ of the three electron, double quantum dot system under the adiabatic ramp pulses by a master equation [2, 3]

DOI: 10.1038/NNANO.2014.336

$$\dot{\rho} = -\frac{i}{\hbar}[H, \rho], \tag{S2}$$

By solving Eqn. (S2) numerically, we obtain the time-evolved density matrix after a detuning ramp over 4 ns for initializaton or 2 ns for measurement (ρ_{ramp}) and we compare the result with the density matrix corresponding to the ground (first excited) state of the system ρ_{g} for the initialization (measurement) sequence. We find that the state fidelity defined by $Tr(\rho_{\mathrm{ramp}}\rho_{\mathrm{g}})$ is higher than 99.99% for both the initialization and the measurement sequences, which shows that infidelity arising from nonadiabaticity during the detuning ramps is negligible.

B. Numerical calculation of infidelity from charge relaxation.

In this subsection we present our characterization of the infidelity arising from charge relaxation during the adiabatic ramps. Charge relaxation does not affect the fidelity of the initialization into state $|0\rangle$, but it does affect the transformation from $|1\rangle$ to $|R\rangle$, which is used for readout.

Our calculations take into the account that the charge relaxation time T_1 depends strongly on detuning. Figure S2 shows the measured T_1 as a function of detuning away from the sweet spot $\delta\varepsilon$, obtained using the pulse sequence shown in the inset to the Fig.S2: the state $|1\rangle$ is prepared at the sweet spot using an X_π rotation, the detuning is then pulsed by an amount $\delta\varepsilon$ and held there for a wait time t_{e} before ramping to the readout point. A fit of the signal amplitude as a function of the wait time t_{e} to an exponential form yields the charge relaxation time T_1, which has a strong dependence on $\delta\varepsilon$. The charge relaxation time T_1 is shortest ($\sim$7 ns) at the sweet spot. Such strong detuning dependence of T_1 has been observed previously in a one-electron Si/SiGe double quantum dot [4].

To estimate the effect of charge relaxation on the readout fidelity, we consider the differential equation governing relaxation from the higher energy to the lower energy state at a detuning $\delta\varepsilon$:

$$\frac{dn_+(\delta\varepsilon, t)}{dt} = -n_+(\delta\varepsilon, t)/T_1(\delta\varepsilon)\ , \tag{S3}$$

where $n_+(\delta\varepsilon, t)$ is the probability of occupation of the higher energy state. We discretize the total measurement ramp time of 2 ns in steps of about 0.2 ns, corresponding to the time spent at each of the $\delta\varepsilon$ data points shown in Fig.S2, and we estimate $n_+(2\ \mathrm{ns}) \approx e^{-0.2/T_1(1.8)} e^{-0.2/T_1(1.6)} \ldots e^{-0.2/T_1(0)} \approx 0.92$.

Since infidelities arising from nonadiabaticity are $<$ 0.01%, the measurement fidelity in the present experiment is limited by charge relaxation around the sweet spot. Taking into account the charge relaxation during the adiabatic ramp used for measurement, we estimate the measurement fidelity itself is about 92%. We note that the relatively short charge relaxation time near the sweet spot may also affect the coherence time of the qubit.

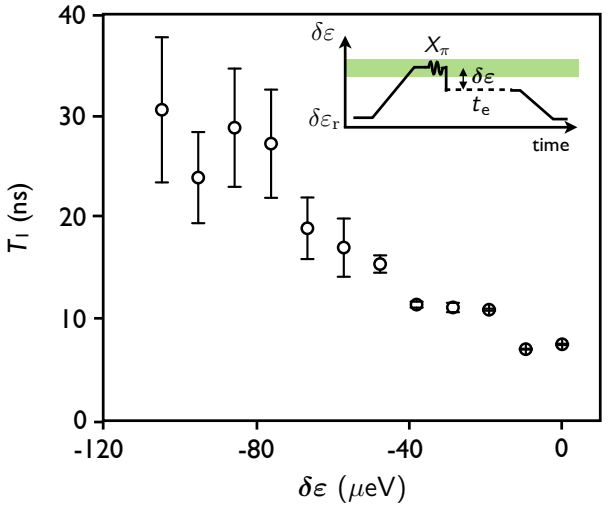

Supplementary Fig. S2. Main panel: Measured charge relaxation time T_1 as a function of detuning from the sweet spot, $\delta\varepsilon$. Inset: Schematic of the pulse sequence used for the measurement.

S3. Z-AXIS ROTATIONS AWAY FROM THE SWEET SPOT

In order to directly compare Ramsey fringes (Z-axis rotations) performed at various detunings we used the pulse sequence shown in Fig. S3a, where the state preparation and measurement axis projection is performed at the sweet spot using $X_{\pi/2}$ rotations, while free evolution takes place at detunings away from the sweet spot using abrupt pulses having amplitude of $\delta\varepsilon$ measured with respect to ε_0. Figure S3b and c shows the resultant Z-axis rotations as a function of $\delta\varepsilon$ and the free evolution time t_{e} and line-cuts of P_1 at several detunings labeled in the legend. The result clearly shows a rapid decrease in T_2* to of order 100 ps when the Z-axis rotation is performed away from the sweet spot.

S4. STATE AND PROCESS TOMOGRAPHY

A. Details of the linear-inversion gate set tomography experiments

Gate set tomography (GST) is a method for self-consistently characterizing state preparation, measurement, and quantum operations. Our method is described in detail in Ref. [5] (Ref. [6] demonstrated a similar protocol); this section discusses some specific issues encoun-

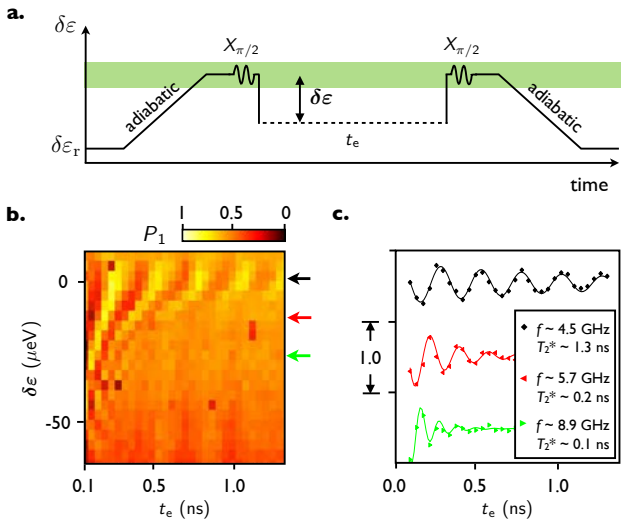

Supplementary Fig. S3. **a**, Schematic pulse sequence used for measurement of Z-axis rotations performed at various detunings. State preparation and measurement axis projection are done at the sweet spot ($\delta\varepsilon \approx 0$) using $X_{\pi/2}$ rotations. **b**, P_1 as a function of detuning variation away from the sweet spot $\delta\varepsilon$ and free evolution time t_e. **c**, Line-cuts of P_1 at $\delta\varepsilon \approx 0$ μeV (black), $\delta\varepsilon \approx -15\mu$eV (red), and $\delta\varepsilon \approx -30\mu$eV (green), which shows a rapid decrease in T_2* when the Z-axis rotation is performed away from the sweet spot.

tered in this experiment.

Like standard QPT, GST requires an *informationally complete* set of measurements – i.e., at least one linearly independent probability per gateset parameter. But it eliminates standard QPT's need for known initialization and measurement processes by doing initialization and measurement with unknown operations selected from the *gateset* to be characterized. Informational completeness is achieved by using fiducial sequences ($\mathcal{F} = \{F_i\}$) built from the gates themselves to generate at least $d^2 = 4$ distinct input states, and to rotate the final state into at least $d^2 = 4$ distinct measurement bases. However, whereas in standard QPT informational completeness can be ensured in advance, in GST we do not know in advance what operations the F_i will perform. Instead, we test the *data* for the signature of informational completeness, and if necessary adjust the fiducial sequences. This signature is the spectrum of the Gram matrix G defined by $G_{i,j} = P_1(F_i F_j)$. G should have rank d^2 if the fiducials $\mathcal{F}$ are informationally complete for a d-dimensional system. In the experiments reporte here, our initial choice of $\mathcal{F}$ accidentally produced a Gram matrix with only three significant eigenvalues; we adjusted the fiducial sequences to ensure that all four eigenvalues of G were large (≥ 0.19). With our initial microwave-pulse gates, chosen to roughly approximate $\pi/2$ rotations, the fiducial set $\mathcal{F} = \{\emptyset, G_1, G_2, {G_1}^2\}$ yielded a Gram matrix with smallest eigenvalue of 0.05, which caused the linear inversion GST to be ill-conditioned. Changing the fourth fiducial to $F_4 = G_1^3$ as well as reducing the rotation angle by changing the amplitude of the ac driving yielded a Gram matrix with smallest eigenvalue 0.19, which ensures reliable linear inversion for the first step of GST. As is shown in Fig. 4c of the main text, GST estimates the rotation angles of G_1, G_2, and G_3 to be 0.38π, 0.41π, and 0.45π, respectively.

B. Details of the non-linear gate set tomography refinement

GST proceeds in two steps: a linear inversion step, where we obtain coarse estimates of the gates, followed by a refinement step. Higher accuracy is attained by performing longer sequences of gates. In this experiment, we performed (and estimated the measurement probability associated with) sequences of the form $F_i G_k^n F_j$, for $i, j = 1 \ldots 4$, $k = 1 \ldots 3$, and $n = 2 \ldots 32$. Many repetitions amplify over/under-rotation error (e.g. by an angle θ) in each gate G_k, so that by measuring $n\theta$ to reasonable accuracy we achieve a very accurate estimate of θ. However, because the associated measurement probabilities are highly nonlinear in G_k, we cannot use linear inversion. Instead, we estimated the gateset $\mathcal{G} = \{\hat{G}_k, \hat{\rho}, \hat{\mathcal{M}}\}$ by maximizing the likelihood $\mathcal{L}(\mathcal{G}) = \Pr(\text{data}|\mathcal{G})$. Since the likelihood function $\mathcal{L}(\mathcal{G})$ is in general nonconvex, we used the linear inversion estimate as a starting point for local optimization. We found that in this case the best local optimization procedure (resulting in the highest maximum likelihood) was to repeatedly apply the Nelder-Mead downhill simplex method until it converged. Since the resulting estimate is not necessarily a physically valid gateset (those for which ρ and $\mathcal{M}$ are valid quantum states/measurements, and each G_k is a completely positive, trace-preserving map), it is projected onto the space of valid gatesets to produce a final estimate. This final maximum-likelihood estimate predicts count statistics that fit the observed data well, but the variability of results with different local optimization procedures indicates that the likelihood contains a number of local minima and suggests that even in our best case the likelihood may not have been strictly maximized. However, this effect appears to be less significant than non-Markovian noise effects, which are not accounted for in GST (unlike QPT, GST can incorporate data from experimental sequences in which a single gate G_k appears more than once – but it does so by explicitly assuming that G_k applies the same quantum process each time it is applied, with no systematic variation with respect to time or context).

C. Standard quantum process tomography (QPT)

We perform standard process tomography on our qubit in the usual way, by preparing precalibrated, informationally complete states, applying the unknown operation to be characterized, and measuring in a precalibrated,

DOI: 10.1038/NNANO.2014.336

informationally complete basis. In our experiment, the state preparation and measurement processes are precalibrated using Rabi oscillation and Ramsey fringe experiments, as detailed in the main text. We perform QPT to characterize a total of four processes: $X_{\pi/2}$, $Z_{\pi/2}$ (shown in Fig. 4a in the main text), and G_1 and G_3 (shown in Fig. 4b in the main text). In all cases, first we initialize to the $|L\rangle$ state, then adiabatically transition to the $|0\rangle$ state, as detailed in the main text. Next, we prepare an informationally complete set of inputs in two separate ways. First, for the $X_{\pi/2}$ and G_1 (which is X-like) operations, we apply the operations $X_{\pi/2}Z_{\pi/2}$ and X_Φ for three separate angles Φ. This gives the $|-X\rangle$ state, in addition to three states that lie on the $y-z$ plane, forming an informationally complete set. Second, for the $Z_{\pi/2}$ and G_3 (which is Z-like) operations, we either do nothing or apply the operations $Z_\Phi X_{\pi/2}$ for three separate angles Φ. This gives for our inputs the states $|0\rangle$ and three states in the $x-y$ plane, which are again informationally complete. The reference time which sets Φ is varied in the experiment and the results with 10 different Φ were used to estimate statistical average and standard deviation of the process matrices and fideltities. We choose these two different input sets for X or Z-gate process tomography for data post-processing convenience. After preparing the informationally complete input set, we then implement the processes to be characterized. Finally, we perform $-Y_{\pi/2}$, $X_{\pi/2}$, and identity operations, followed by a measurement in the Z-basis. Note that in the state tomography of X-gate we implement tomography in the rotating frame by adjusting phase of the measurement $\pi/2$ pulses taking phase accumulation during manipulation pulse into account, whereas Z-gate tomography is performed in the lab frame where the phase of the measurement pulses are fixed. Once these measurements are complete, we use maximum-likelihood estimation [1, 7, 8] to reconstruct the χ matrix representation of the unknown process, given by [7, 8]

$$\mathcal{E}(\rho) = \sum_{m,n=1}^{4} \tilde{E}_m \rho \tilde{E}_n^\dagger \chi_{mn}, \tag{S4}$$

where $\mathcal{E}(\rho)$ is the density matrix specifying the output for a given input density matrix ρ, $\tilde{E}_m$ are the basis operators in the space of 2×2 matrices, and χ is the process matrix. The entries of this matrix are plotted in Fig. 4a of the main text.

[1] Kim, D. *et al.* Quantum control and process tomography of a semiconductor quantum dot hybrid qubit. *Nature* **511**, 70–74 (2014).

[2] Shi, Z. *et al.* Fast coherent manipulation of three-electron states in a double quantum dot. *Nature Comm.* **5**, 3020 (2014).

[3] Shi, Z. *et al.* Coherent quantum oscillations and echo measurements of a si charge qubit. *Phys. Rev. B* **88**, 075416 (2013).

[4] Wang, K., Payette, C., Dovzhenko, Y., Deelman, P. W. & Petta, J. R. Charge relaxation in a single-electron Si/SiGe double quantum dot. *Phys. Rev. Lett.* **111**, 046801 (2013).

[5] Blume-Kohout, R. *et al.* Robust, self-consistent closed-form tomography of quantum logic gates on a trapped ion qubit (2013). Preprint arXiv:1310.4492.

[6] Merkel, S. T. *et al.* Self-consistent quantum process tomography. *Phys. Rev. A* **87**, 062119 (2013).

[7] Nielsen, M. A. & Chuang, I. L. *Quantum Computation and Quantum Information* (Cambridge University Press, Cambridge, 2000).

[8] Chow, J. M. *et al.* Randomized benchmarking and process tomography for gate errors in a solid-state qubit. *Phys. Rev. Lett.* **102**, 090502 (2009).